$Revision: 1.7 $
$Date: 2002/02/04 16:50:04 $

last modification: February 4, 2002
to appear in "Computational Materials Science"
URL: http://magnet.atp.tuwien.ac.at/scholz/projects/papers/pub_scholz.html

Micromagnetic Simulation of Domain Wall Pinning and Domain Wall Motion

W. Scholz, H. Forster, D. Suess, T. Schrefl, and J. Fidler

Institut für Angewandte und Technische Physik, Vienna University of Technology, Wiedner Hauptstraße 8-10/137, A-1040 Vienna, Austria

Abstract

Domain wall pinning is the coercivity mechanism of permanent magnets used in high temperature applications. In SmCo based magnets domain walls get trapped at the cellular precipitation structure causing a high coercive field. The motion of domain walls and their propagation velocity are important in soft magnets as used in sensor applications. A finite element micromagnetic algorithm was developed to study the motion of domain walls in complex microstructures. The cellular microstructure of SmCo magnets or the cylindrical soft wires can be easily built using tetrahedral finite elements. The pinning of the domain walls has been studied for different material compositions. Attractive and repulsive domain wall pinning are observed and their behaviour for increasing thickness of the precipitation structure is explained.

The motion of domains in magnetic nanowires was calculated using adaptive mesh refinement. The wall velocity strongly depends on the domain wall structure. Transverse and vortex walls have been observed and their velocity in wires of different thickness has been studied.

Corresponding author

Werner Scholz

Vienna University of Technology

Institute of Applied and Technical Physics

Wiedner Hauptstraße 8-10/137

A-1040 Vienna

Austria

tel: +43 1 58801 13729

fax: +43 1 58801 13798

email: werner.scholz@tuwien.ac.at

1 Introduction

Magnetic domain walls are a key feature of ferromagnetic materials and their behaviour determines the properties and performance, which are exploited in many applications. They separate different regions of uniform magnetization and these magnetic domains can shrink and expand by moving the domain walls.

The performance of permanent magnets is characterized by the coercive field, for example. If only a small external magnetic field is required to nucleate a domain of reversed magnetization and move the domain wall through the magnet, it has a low coercive field and is referred to as magnetically soft. However, if there is some kind of hindrance to the motion of domain walls, the coercive field is increased and the material becomes interesting as a permanent magnet.

This mechanism is called "domain wall pinning" and Samarium-Cobalt type permanent magnets, which have been discovered in the 1960's by Strnat and coworkers [1], are a well known example for "pinning controlled" magnets [2, 3]. Their excellent magnetic properties are due to the high magnetic moment of Sm and Co as well as the high magnetocrystalline anisotropy. The high Curie temperature of 720 °C for $SmCo_5$ and 820 °C for Sm_2Co_{17} [4] makes it the best material currently available for high temperature magnets [5, 6, 7]. The micromagnetic model, which has been used for our simulations, is described in section 2 and the results are discussed in section 3.

Domain walls in magnetic nanowires are also a key feature of magneto-

electronic devices and magnetic sensors based on the magnetoresistive effect. We have studied their behaviour in Co nanowires using adaptive mesh refinement [8]. The nucleation of reversed domains and their expansion by domain wall motion is calculated by solving the Gilbert equation of motion, which is explained in section 2. Two different types of domain walls have been found for different wire diameters and the velocity of the walls is strongly influenced by the damping constant. These results are presented in section 4.

2 Finite Element Micromagnetics

In this work the domain wall pinning and the the domain wall motion were calculated using a hybrid finite element / boundary element technique.

The simulation of dynamic domain wall processes must take into account gyromagnetic precession of the magnetic polarization vector $\mathbf{J}$ in the effective field $\mathbf{H}_{\text{eff}}$ and damping. The effective field is given by the variational derivative $\mathbf{H}_{\text{eff}} = -\delta E_{\text{t}}/\delta \mathbf{J}$ of Gibbs' free energy

$$E_t = \int \left[A \sum_{i=1}^{3} (\nabla \beta_i)^2 - K_u (\mathbf{u} \cdot \beta)^2 - \frac{1}{2} \mathbf{J} \cdot \mathbf{H}_{\text{d}} - \mathbf{J} \cdot \mathbf{H}_{\text{ext}} \right] dV \quad . \tag{1}$$

We have taken into account the contributions of exchange energy (A denotes the exchange constant and β_i the direction cosines of the magnetic polarization vector), magnetocrystalline anisotropy energy (K_{u} is the magnetocrystalline anisotropy constant and $\mathbf{u}$ the anisotropy axis), magnetostatic energy (the magnetostatic field $\mathbf{H}_{\text{d}}$ is calculated using a scalar potential) and Zeeman energy.

The boundary conditions for the interfaces between regions with different magnetic properties [9, 10, 11] are implicitly included in the effective field. Thus, they need no special attention during the time integration.

The time evolution of the magnetic polarization is described by the Gilbert equation of motion

$$\frac{\partial \mathbf{J}}{\partial t} = -|\gamma| \mathbf{J} \times \mathbf{H}_{\text{eff}} + \frac{\alpha}{J_{\text{s}}} \mathbf{J} \times \frac{\partial \mathbf{J}}{\partial t} \quad , \tag{2}$$

where the first term describes the gyromagnetic precession in the effective field and the second the damping of the motion.

3 Domain Wall Pinning

With the technique described in the previous section the domain wall pinning in precipitation hardened Sm(Co,Fe,Cu,Zr)$_z$ magnets has been investigated. The magnetic properties of this material are determined by the fine cell morphology of the cellular precipitation structure with rhombohedral cells of $Sm_2(Co,Fe)_{17}$ with a typical diameter of 100-200 nm, which are separated by a boundary phase of Sm(Co,Cu,Zr)$_{5-7}$ [12]. The cellular precipitates act as pinning sites for magnetic domain walls, where their motion is stopped until the external field is increased above the pinning field. This behaviour can be observed in Lorentz electron micrographs [13].

A finite element model of the microstructure of Sm(Co,Fe,Cu,Zr)$_z$ [14, 15, 16] has been developed. It consists of $2 \times 2 \times 2$ rhombohedral cells with a spacer layer for the cell boundary phase in between (see fig. 1). The edge

length e and the "corner angle" β of the rhombohedrons as well as the thickness t of the precipitation are variable. The "space diagonal" D, is parallel to the easy axis. The domain wall of the initial magnetization distribution of our simulations lies in the plane, which is indicated by the thick lines, and separates two antiparallel magnetic domains with their magnetization parallel to the easy axis.

The difference in composition and crystal structure between the cells and the cell boundary phase gives rise to a difference in the magnetocrystalline anisotropy. As a result it is energetically favorable for a magnetic domain wall to either stay in the cell boundary phase ("attractive domain wall pinning" if the domain wall energy is lower) or just inside the cells ("repulsive domain wall pinning" if the domain wall energy in the cell boundary phase is higher than that in the cells) [17].

The following material parameters for 300 K [4] have been assumed: For the cells ("2:17" type) $J_s = 1.32$ T, $A = 14$ pJ/m, $K_1 = 5$ MJ/m^3. For the cell boundary phase ("1:5" type) we have used $J_s = 0.8$ T, $A = 14$ pJ/m, $K_1 = 1.9$ MJ/m^3. Thus, the exchange length is 1.7 nm in the cells and 2.7 nm in the cell boundary phase. The resulting domain wall width is 5.3 nm in the cells and 8.5 nm in the cell boundary phase.

By varying the anisotropy constant K_1 of the precipitation between 0.4 MJ/m^3 (to mimic almost isolated cells or a close to paramagnetic - Cu rich - intercellular phase, A and J_s have also been reduced) and the value for the cells we have studied the influence of the material parameters. The demagnetization curves in figure 2 have been obtained for cells with $e = 50$ nm

and $\beta = 60°$, which gives $D \approx 125$ nm, and $t = 5$ nm. The strongest pinning effect is found for very low values of the anisotropy constant in the intercellular phase (horizontal plateau in the demagnetization curve in figure 2). As K_1 approaches the value for the cells (2:17 phase) the pinning effect disappears.

"Repulsive pinning" is found, if the magnetocrystalline anisotropy of the intercellular phase is larger than that of the cells.

The demagnetization curves for repulsive pinning and different values of the anisotropy constant of the intercellular phase are shown in figure 3. For only slightly enhanced values of the anisotropy constant K_1 we find no pinning, but for $\Delta K_1 \geq 4.0$ MJ/m^3 the pinning field reaches 1.5 kA/m. In this regime the pinning field is directly proportional to ΔK_1. This linear behaviour has also been predicted by Kronmüller [18]. In figure 4 the results for attractive and repulsive pinning are summarized.

The thickness of the intercellular phase also has an important influence on the pinning mechanism and the pinning fields.

The thickness has been varied from $t = 10$ nm to $t = 40$ nm and an anisotropy constant of $K_1^{\mathrm{attr}} = 1.2$ MJ/m^3 and $K_1^{\mathrm{rep}} = 9$ MJ/m^3 have been assumed for the intercellular phase for the cases of attractive and repulsive pinning, respectively.

For very thin intercellular phases the effect of attractive domain wall pinning is lost, because the domain wall does not "fit into" the precipitation phase. Thus, the domain wall moves through the magnet without any hindrances. As the thickness of the intercellular phase increases, the pinning field increases (cf. fig. 5). However, for very thick intercellular phases, the

pinning field decreases again. Figure 6 shows the reason for this behaviour: The domain wall bends into the precipitation phase, which leads to high stray fields at the corners of the cells and facilitates the reversal of magnetization in the cells. For a thickness of more than 40 nm of the intercellular phase, the pinning behaviour is lost again, because the domain wall sweeps through the whole intercellular phase and reverses its magnetization. As a result the unreversed cells remain until nucleation starts the reversal of their magnetization.

In the case of repulsive domain wall pinning, a minimum thickness of the intercellular phase is required, too. However, in this regime the pinning field strongly increases for increasing thickness until it reaches a maximum level, which is shown in figure 5. Once again, the sharp corners of the cells play an important role, because this is the place, where the domain wall can cross the intercellular phase (cf. fig. 7). As the thickness of the intercellular phase increases, the energy barrier becomes wider and this mechanism gets more and more difficult.

4 Domain Wall Velocity

In permanent magnet applications it is important to hinder the motion of domain walls and pin them at precipitates or defects to obtain a high coercive field. In magnetic-electronic devices and sensors the nucleation and propagation of domain walls determines their speed and performance. Thus, we study the same physical object, a magnetic domain wall, but now we are

interested in its dynamic behaviour.

We have assumed a Co nanowire of a length of 500 nm with uniaxial magnetocrystalline anisotropy parallel to the long axis of the wire and an additional soft magnetic end of 100 nm, which is required to nucleate a reverse domain and hereby inject the domain wall. The material parameters are $J_\mathrm{s} = 1.76$ T, $A = 1.3 \times 10^{-11}$ J/m and $K_\mathrm{u} = 4.5 \times 10^5$ J/m^3 [19]. Our finite element micromagnetic model has been modified to adaptively refine the mesh in regions of interest, which was around the domain wall. The algorithm is described in detail in [8].

The structure of the domain wall and its velocity strongly depend on the diameter d of the nanowire and the damping constant. For $d < 20$ nm a "transverse wall" (fig. 8) [20] is found, because it minimizes the exchange energy, which is the dominant contribution, at the expense of magnetostatic energy due to surface charges. With increasing diameter of the wire, the magnetostatic energy becomes more important. Thus, for $d > 20$ nm a "vortex wall" (fig. 8) is observed: In its center a vortex with the symmetry axis parallel to the axis of the wire is formed, which reduces the magnetic stray fields and the magnetostatic energy at the expense of exchange energy.

For the critical diameter of $d = 20$ nm both walls are found. Figure 9 gives the wall velocities for different wire diameters. The open symbols indicate transverse walls and the filled symbols indicate vortex walls.

The damping constant α in the Gilbert equation of motion (eq. 2) has a strong influence on the domain wall velocity, which is markedly different for the two different types of domain walls. For $d = 10$ nm only transverse

domain walls are formed and figure 10 shows its velocity for different damping constants. With increasing damping constant the velocity increases from 50 m/s for $\alpha = 0.05$ to 520 m/s for $\alpha = 1$ at an applied field of 500 kA/m. For higher damping constants the domain wall velocity increases faster for higher external fields. In the transverse wall gyromagnetic precession is the driving force of the motion.

For a wire with $d = 40$ nm a vortex wall is observed and its velocity for different damping constants is given in figure 11. The domain wall velocity increases with decreasing damping constant, reaching 2000 m/s for $d = 40$ nm, $\alpha = 0.05$ and an applied field of 250 kA/m. A similar behaviour has been found with simple analytical models for Bloch-type domain walls [21]. However, a detailed analysis of the magnetization distribution during the motion of the domain wall reveals, that the vortex does not remain in the middle of the wire. Its core moves towards the surface perpendicular to the axis of the wire. As it vanishes on one side another vortex is formed on the opposite side due to the strong stray fields. Thus, the motion of the vortex domain wall consists in a repeated formation and vanishing of vortices. The increase of the vortex domain wall velocity with decreasing damping constant is expected in Bloch type walls [22]. Vortex walls achieve higher velocities than transverse walls due to the more Bloch-like character leading to a higher mobility of the wall [23].

5 Conclusions

We have studied the behaviour of magnetic domain walls using numerical micromagnetic simulations. The pinning effect in precipitation hardened SmCo magnets showed the influence of intercellular phases on the domain wall propagation. Depending on the material composition attractive and repulsive pinning has been observed and the influence of the thickness of the intercellular phase has been studied. The dynamics of domain wall motion have been studied in Co nanowires, and again the importance of the thickness of the wire has been shown. Two different types of domain walls have been found and their propagation speed has been investigated.

Work supported by the EC COST Action P3, EC project HITEMAG (GRD1-1999-11125) and the Austrian Science Fund (Y-132 PHY).

References

[1] Strnat, K. J., Hoffer, G., Oson, J., and Ostertag, W., *J. Appl. Phys.*, **38**, 1001–1002 (1967).

[2] Strnat, K. J., "Rare earth-cobalt permanent magnets", in *Ferromagnetic Materials*, edited by E. P. Wohlfarth and K. H. J. Buschow, North-Holland, 1988, vol. 4, pp. 131–209.

[3] Durst, K. D., and Kronmüller, H., "Magnetic hardening mechanisms in sintered Nd-Fe-B and Sm(Co, Cu, Fe, Zr)$_{7.6}$ permanent magnets", in *Proceedings of the Eighth International Workshop on Rare-Earth Magnets and their Applications and the Fourth International Symposium on Magnetic Anisotropy and Coercivity in Rare Earth-Transition Metal Alloys*, edited by K. J. Strnat, Univ. Dayton, Dayton, OH, USA, 1985, pp. 725–735.

[4] Durst, K.-D., Kronmüller, H., and Ervens, W., *phys. stat. sol. (a)*, **108**, 403–416 (1988).

[5] Walmer, M. S., Chen, C. H., and Walmer, M. H., *IEEE Trans. Magn.*, **36**, 3376–3381 (2000).

[6] Corte-Real, M., Chen, Z., Okumura, H., and Hadjipanayis, G., *IEEE Trans. Magn.*, **36**, 3306–3308 (2000).

[7] Liu, S., Yang, J., Doyle, G., Potts, G., and Kuhl, G. E., *Journal of Applied Physics*, **87**, 6728–6730 (2000).

[8] Forster, H., Schrefl, T., Suess, D., Scholz, W., Tsiantos, V., Dittrich, R., and Fidler, J., *J. Appl. Phys.* (2002), in print - MMM'01 paper no. AF-02.

[9] Skomski, R., and Coey, J. M. D., *Phys. Rev. B*, **48**, 15812–15816 (1993).

[10] Skomski, R., Zeng, H., and Sellmyer, D. J., *IEEE Trans. Magn.*, **37**, 2549–2551 (2001).

[11] White, R., *An Introduction to the Finite Element Method with Applications to Nonlinear Problems*, John Wiley and Sons, New York, 1985.

[12] Kronmüller, H., "Nucleation and propagation of reversed domain in RE-Co-magnets", in *Proceedings of the 6th International Workshop on Rare Eart-Cobalt Permanent Magnets and Their Applications and 3rd International Symposium on Magnetic Anisotropy and Coercivity in Rare Earth-Transition Metal Alloys*, edited by J. Fidler, Tech. Univ. Vienna, Vienna, Austria, 1985, pp. 555–565.

[13] Hadjipanayis, G. C., Tang, W., Zhang, Y., Chui, S. T., Liu, J. F., Chen, C., and Kronmüller, H., *IEEE Trans. Magn.*, **36**, 3382–3387 (2000).

[14] Fidler, J., Skalicky, P., and Rothwarf, F., *IEEE Trans. Magn.*, **19**, 2041–2043 (1983).

[15] Mishra, R. K., Thomas, G., Yoneyama, T., Fukuno, A., and Ojima, T., *J. Appl. Phys.*, **52**, 2517–2519 (1981).

[16] Rabenberg, L., Mishra, R. K., and Thomas, G., *J. Appl. Phys.*, **53**, 2389–2391 (1982).

[17] Tang, W., Zhang, Y., Gabay, A. M., de Campos, M. F., and Hadjipanayis, G. C., *J. Magn. Magn. Mater.* (submitted - JEMS'01 paper no. J-041).

[18] Kronmüller, H., Ervens, W., and Fernengel, W., *IEEE Trans. Magn.*, **MAG-20**, 1569–1571 (1984).

[19] Yang, W., Lambeth, D. N., and Laughlin, D. E., *J. Appl. Phys.*, **87**, 6884–6886 (2000).

[20] McMichael, R. D., and Donahue, M. J., *IEEE Trans. Magn.*, **33**, 4167–4169 (1997).

[21] Schryer, N. L., and Walker, L. R., *Journal of Applied Physics*, **45**, 5406–5421 (1974).

[22] Doering, W., *J. Appl. Phys.*, **39**, 1006 (1968).

[23] Kirk, K. J., Scheinfein, M. R., Chapman, J. N., McVitie, S., Ward, M. F. G. B. R., and Tennant, J. G., *J. Phys. D: Appl. Phys.*, **34**, 160–166 (2001).

Table and figure captions

Fig. 1: Finite element model of the microstructure of a Sm(Co,Fe,Cu,Zr)$_z$ magnet.

Fig. 2: Demagnetization curves for reduced magnetocrystalline anisotropy K_1 of the cell boundary phase (values in the legend in MJ/m^3) - attractive pinning.

Fig. 3: Demagnetization curves for enhanced magnetocrystalline anisotropy K_1 of the cell boundary phase (values in the legend in MJ/m^3) - repulsive pinning.

Fig. 4: Pinning field vs. difference in anisotropy constant between the cells and the cell boundary phase.

Fig. 5: Demagnetization curves for varying thickness t (values in the legend in nm) of the intercellular phase.

Fig. 6: Bending of the domain wall into the intercellular phase (attractive pinning).

Fig. 7: Depinning of the domain wall on the corners of the rhombohedral cells (repulsive pinning).

Fig. 8: Magnetization distribution in a transverse wall (cut plane parallel to the wire axis) and in a vortex wall (cut plane perpendicular to the wire axis through the vortex core).

Fig. 9: Domain wall velocity as a function of the applied field for different wire diameters. The open symbols and the filled symbols refer to transverse and vortex walls, respectively.

Fig. 10: Domain wall velocity of transverse walls for different damping constants for a wire with $d = 10$ nm.

Fig. 11: Domain wall velocity of vortex walls for different damping constants for a wire with $d = 40$ nm (triangles: $\alpha = 0.05$; circles: $\alpha = 1$).

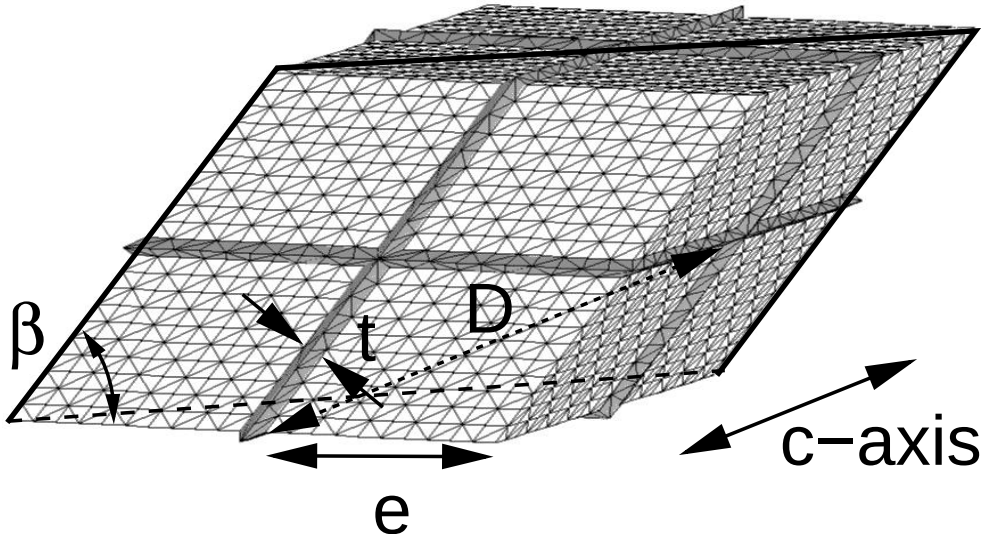

Figure 1: Scholz et al.

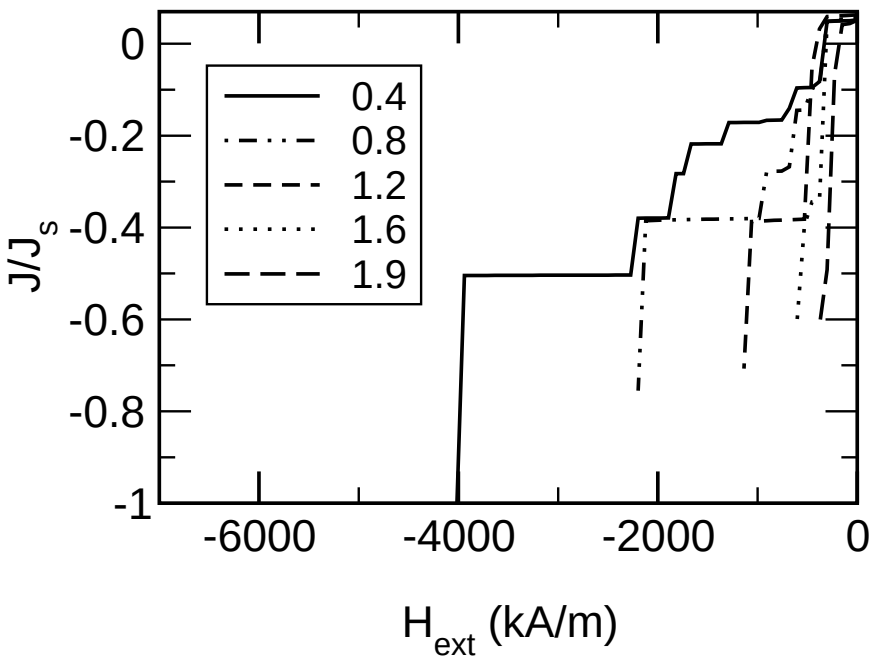

Figure 2: Scholz et al.

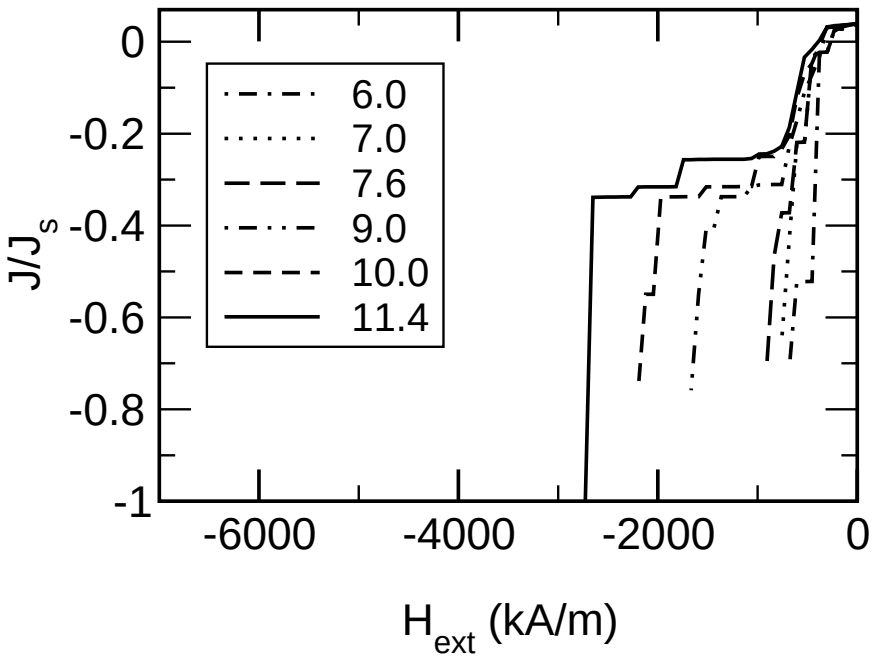

Figure 3: Scholz et al.

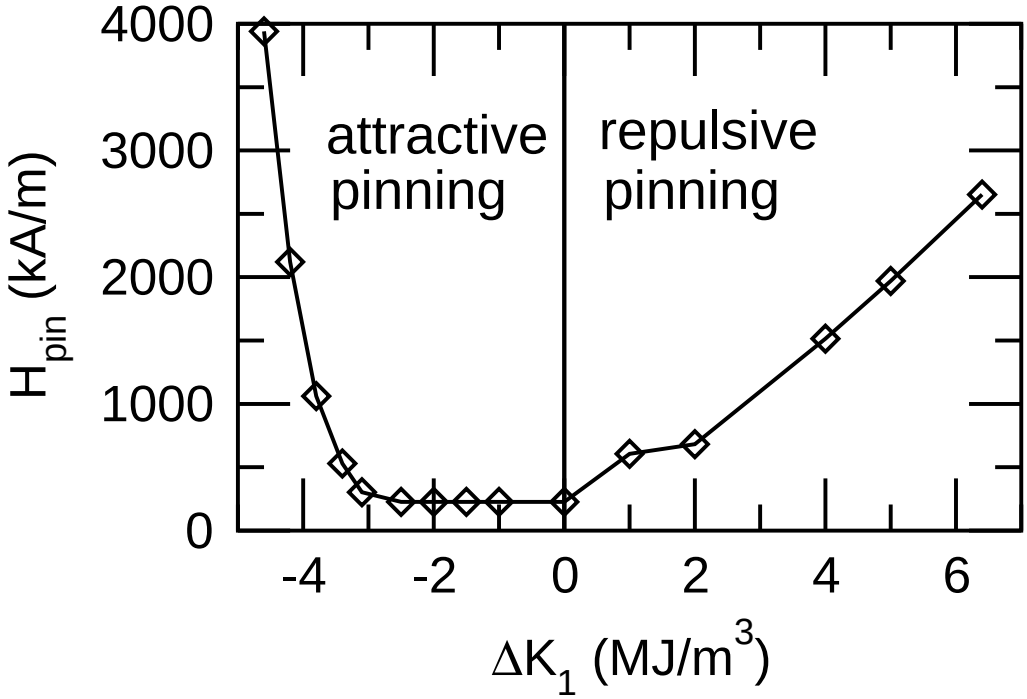

Figure 4: Scholz et al.

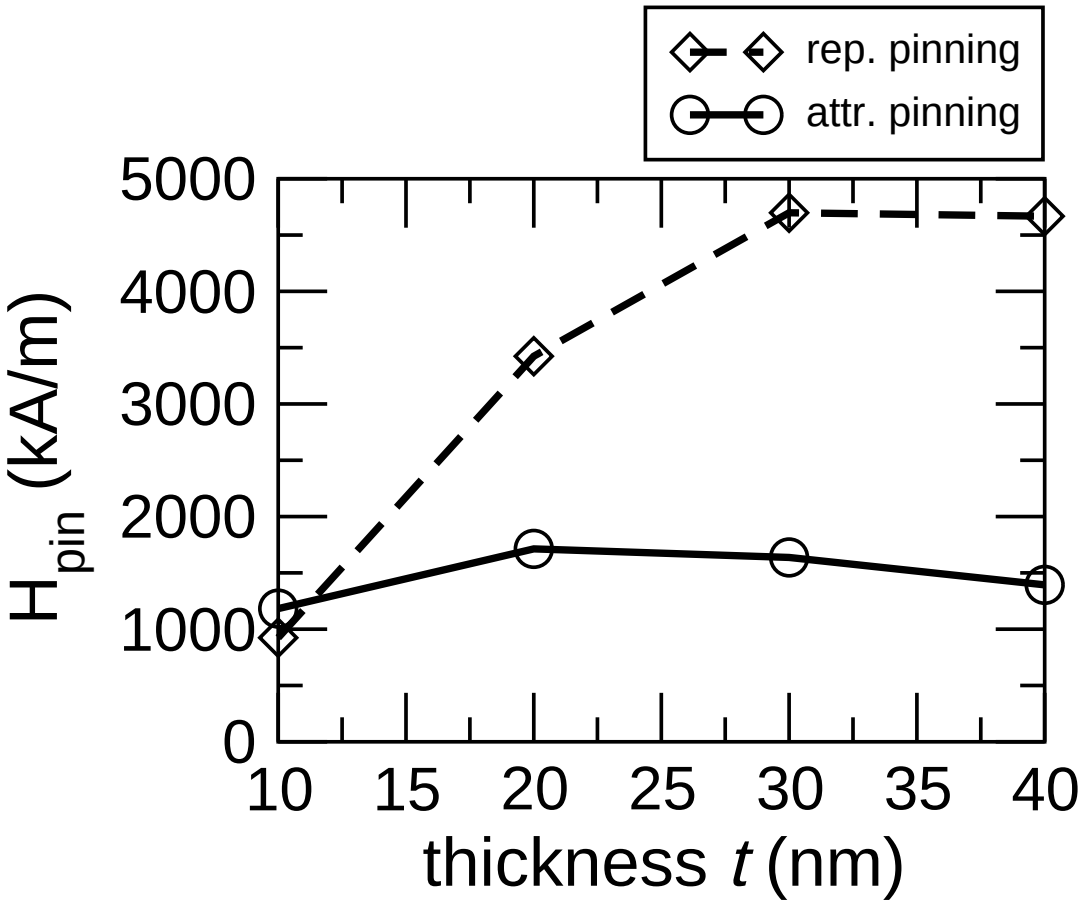

Figure 5: Scholz et al.

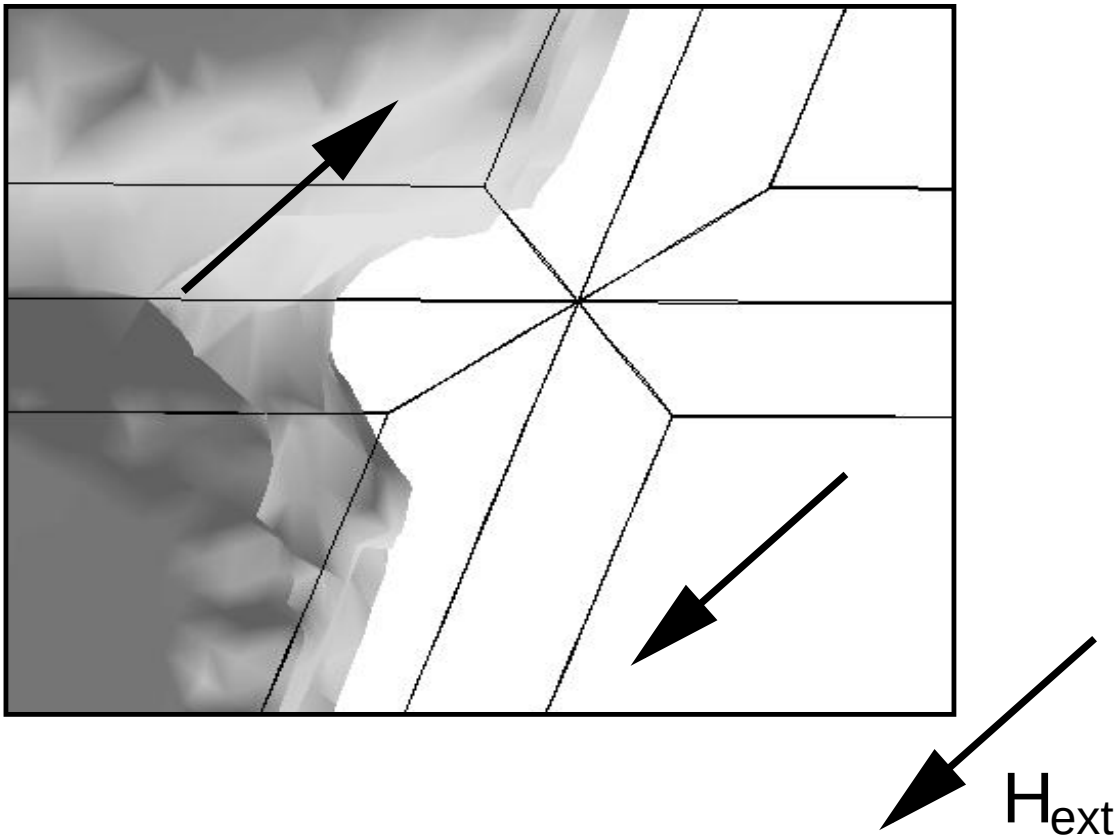

Figure 6: Scholz et al.

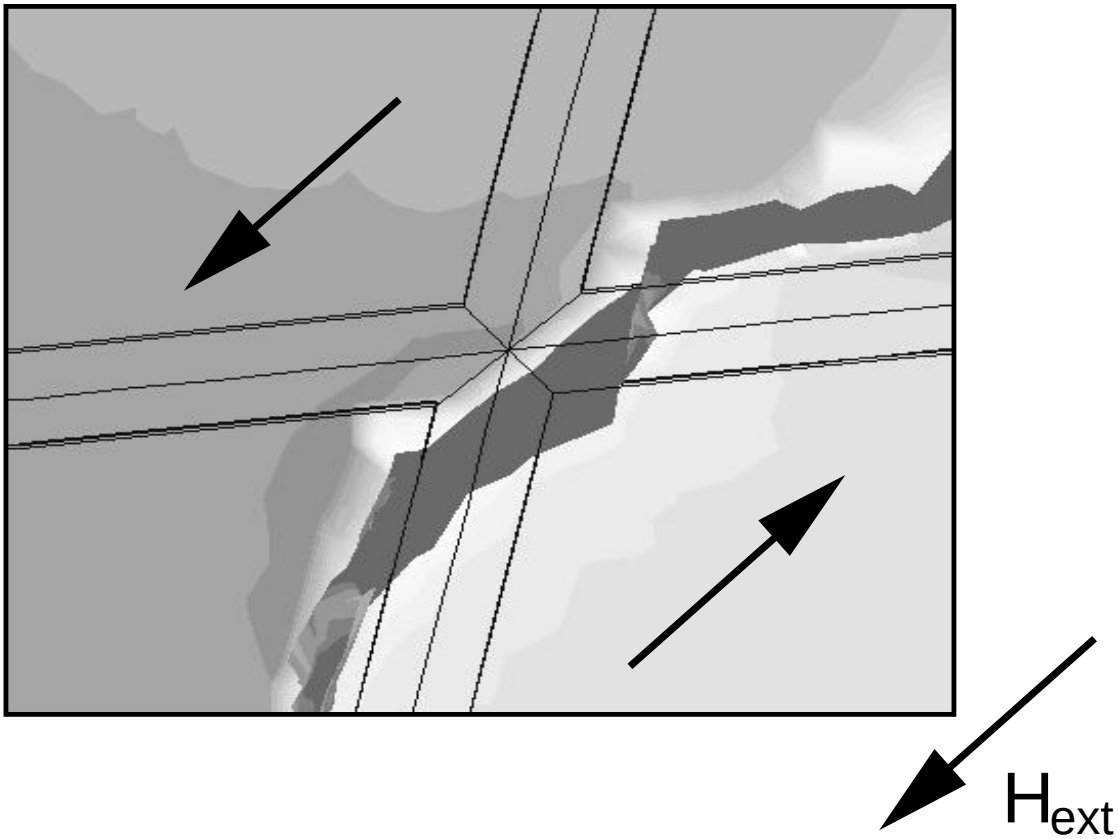

Figure 7: Scholz et al.

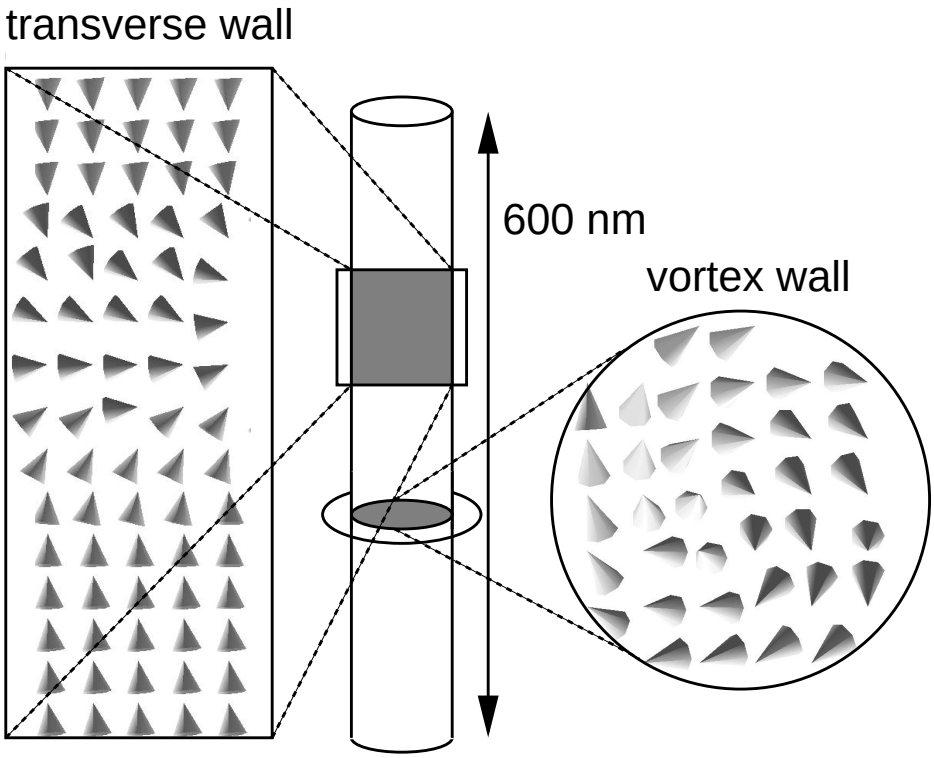

Figure 8: Scholz et al.

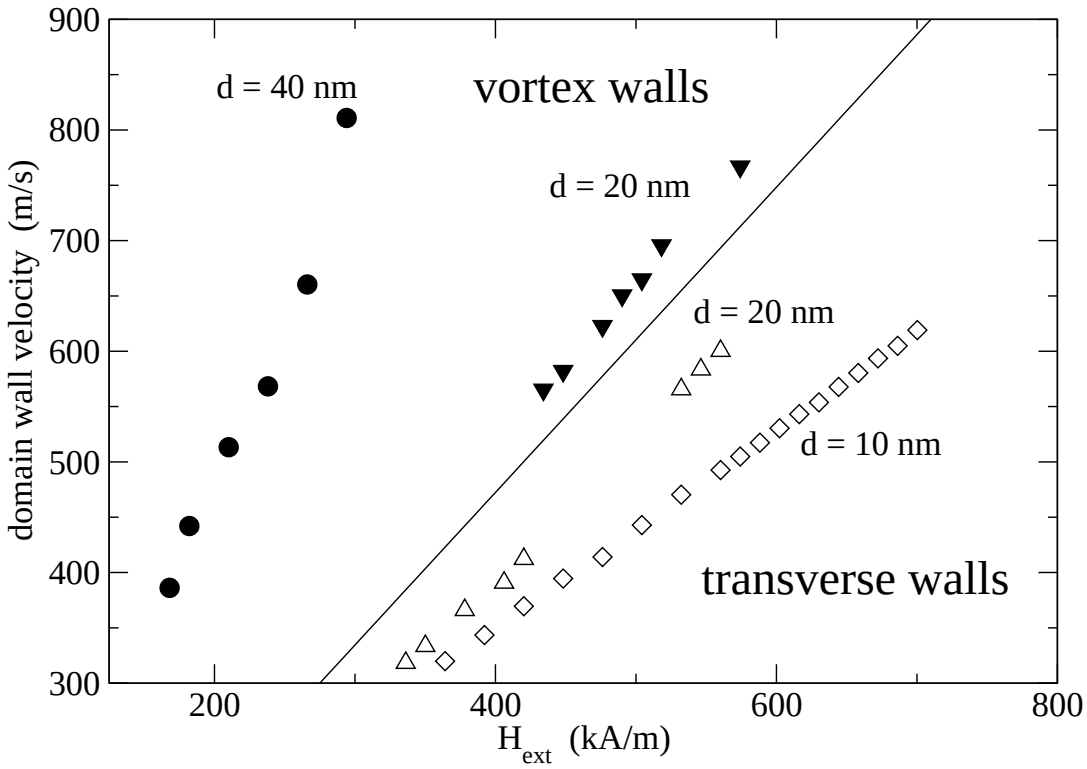

Figure 9: Scholz et al.

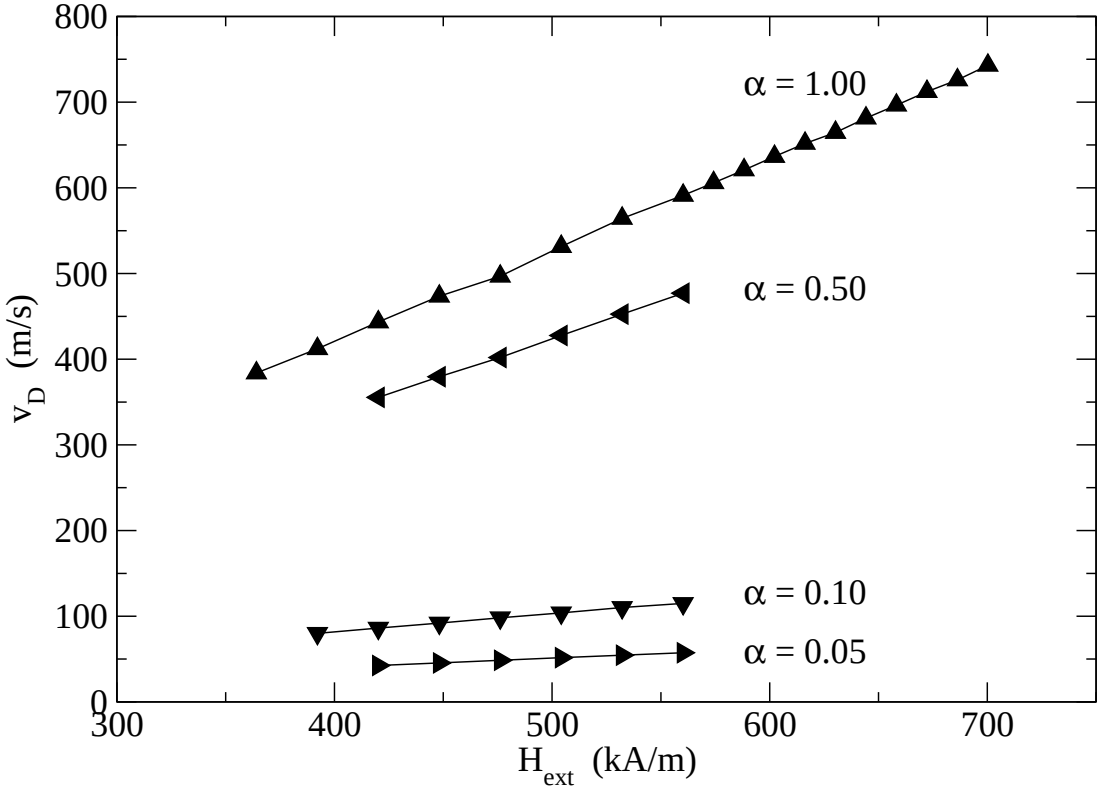

Figure 10: Scholz et al.

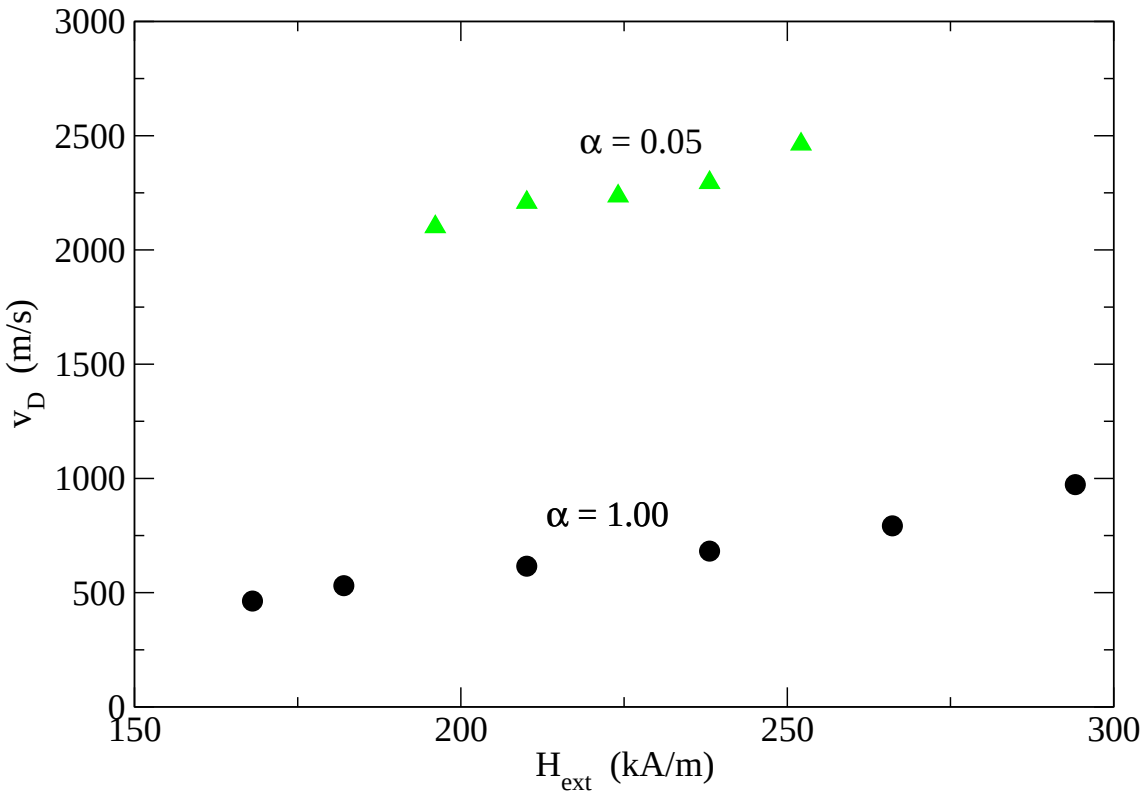

Figure 11: Scholz et al.